JOURNAL OF CATALYSIS 156, 11–18 (1995)

# Hydroisomerization and Hydrocracking of *n*-Heptane on Pt/SAPO-5 and Pt/SAPO-11 Catalysts

J. M. Campelo, F. Lafont, and J. M. Marinas

*Department of Organic Chemistry, Sciences Faculty, Cordoba University, Avda. S. Alberto Magno, s/n, E-14004 Cordoba, Spain*

Received June 13, 1994; revised February 21, 1995

**The activity, stability, and selectivity of a series of bifunctional Pt/SAPO-5 and Pt/SAPO-11 catalysts containing 0.5 wt% platinum were compared for *n*-heptane transformation at 300–450°C and atmospheric and 3 and 5 bars hydrogen pressures. Hydrogen pressure had a strong influence on the activity, *iso*-heptane selectivity, and time-on-stream deactivation. Isomerization of *n*-heptane to *iso*-heptanes was the major reaction with Pt/SAPO-5 catalyst, especially at lower conversions, whereas Pt/SAPO-11 shows high selectivity to isomers in all conversion range. The selectivity patterns found in these classes of molecular sieve catalysts are well interpreted in terms of a series of reaction pathways that incorporate both confinement effects and shape selectivity factors as being important in determining the observed product distribution. Based on experimental results, the protonated cyclopropane appears as an intermediate in the mechanism of this reaction.** © 1995 Academic Press, Inc.

## INTRODUCTION

Environmental considerations have brought about a rapid phaseout of lead additives in gasoline. Since lead is added to gasoline to increase the octane number, other means of achieving this must be employed. Gasoline octane number can be boosted by increasing the catalytic reformer severity (i.e., removing low-octane paraffins), by increasing paraffin alkylation, by adding MTBE (methyl *tert*-butyl ether), and by replacing straight-run tops ($C_5$–$C_7$ paraffins) with isomerized products. Such paraffin isomerization can bring a substantial increase in the octane number; for example, RON (research octane number) for *n*-hexane is 29, but for 2- and 3-methylpentane and 2,2- and 2,3-dimethylbutane RON is 78, 76, 82, and 104, respectively. So *n*-hexane and *n*-heptane have much lower octane numbers than their corresponding branched isomers. In these isomerization processes widespread use is made of bifunctional catalysts containing acidic sites for skeletal isomerization and cracking and metallic sites for hydrogenation/dehydrogenation (1). In addition, when adjacent pairs of acid–base sites are present, cyclization and aromatization reactions are also found. Hydroisomerization is a typical acid-catalyzed reaction and this skeletal isomerization conversion is an equilibrium-limited reaction, where the lower the reaction temperature, the higher the isomerization; this results in high-octane products. A very low reaction temperature (150°C) can be employed by using chloride alumina catalysts containing a noble metal. However, these catalysts suffer from the disadvantage of being quite sensitive to trace impurities in the feed, such as water. In contrast, zeolite-based catalysts have come into wide application because of their enhanced selectivity for desired products via shape selectivity (2). These catalysts are most robust and can withstand low levels of impurities such as sulphur and water in the feedstock. The catalytic characteristics depend also on the reactant; thus the reactivity of *n*-alkanes increases with their chain length while the selectivity for isomerization decreases (3).

A large number of molecular sieves based on aluminophosphates have been synthesized and identified in recent years (4–6). Silicoaluminophosphate (SAPO) molecular sieves have pore structures similar to those of conventional zeolites, but usually with a milder acidity due to the presence of phosphorus (7). The unique combination of pore size variability and somewhat adjustable acidity suggests the potential of SAPO-*n* sieves in many catalytic applications (8–13). For example, in propene oligomerization, *n*-hexane dehydrocyclization, and xylene isomerization, both enhanced selectivities and decreased deactivation rates have been observed for the medium-pore-size silicoaluminophosphate and metalloaluminophosphate (MeAPO) molecular sieves. This was attributed to a combination of mild acidity and shape selectivity. However, little has been reported on the catalytic properties of bifunctional Pt/SAPO. The main objective of the present work is to examine this effect of surface acidity and shape selectivity with both Pt/SAPO-5 and Pt/SAPO-11 using the *n*-heptane hydroconversion as a test reaction. The framework of SAPO-11 is isotopic to that of ALPO-11, with an AEL-type structure. The void volume consists of nonintersecting elliptical 10-membered ring pores of 0.39 × 0.64 nm diameter. The framework of SAPO-5 is isotopic to that of ALPO-5, with an AFI-type structure,



0021-9517/95 $12.00

which has a unidimensional pore system consisting of cylindrical channels bounded by 12-membered rings 0.80 nm in diameter.

## EXPERIMENTAL

### *Catalyst Preparation*

SAPO-5 was prepared by combining 23.06 g of 85 wt% $H_3PO_4$ (Merck) and 82.47 g of water, to which was added 13.81 g of hydrated aluminum oxide (a pseudoboehmite phase, 74.2 wt% $Al_2O_3$ and 25.8 wt% $H_2O$, Vista), and stirring until homogeneous. To this mixture was added a dispersion of 2.59 g of fumed silica (92.8 wt% $SiO_2$ and 7.2 wt% $H_2O$, Aerosil 200, Serva) in 29.41 g of tri-*n*-propylamine (Merck), and this mixture was stirred until homogeneous. The reaction mixture was sealed in a stainless-steel pressure vessel lined with PTFE and heated in an autoclave at 200°C at autogenous pressure for 24 h.

SAPO-11 was prepared by combining 53 g of water and 30.2 g of aluminum isopropoxide (Merck), to which was added 17.1 g of 85 wt% $H_3PO_4$. To this were added 0.47 g of fumed silica and then, after stirring, 7.4 g of di-*n*-propylamine (Merck). The reaction mixture was poured in a PTFE-coated stainless-steel autoclave and heated at 150°C at autogenous pressure for 133 h.

Both solid reaction products were recovered by centrifugation, washed with deionized water, and dried at 120°C overnight. Furthermore, they were calcined in air at 25 to 600°C for 6 h at a program rate of 10°C $min^{-1}$. The chemical composition of the crystalline samples was determined by the ICP method and the results, given in terms of oxide contents, were $(Si_{0.07}Al_{0.45}P_{0.48})O_2$ for SAPO-5 and $(Si_{0.01}Al_{0.45}P_{0.54})O_2$ for SAPO-11.

Metal loading was carried out by wet impregnation with $Cl_2(NH_3)_4Pt$ (Aldrich, 98% purity); a known amount of SAPO-5 or SAPO-11 was added to a concentrated aqueous salt solution containing the amount of metal necessary to obtain the desired weight loading (0.50 wt%). After impregnation for 24 h, the materials were dried in air at room temperature, for at least 48 h, and then at 120°C overnight, and finally were calcined in flowing $O_2$ (60 ml $min^{-1}$) at 400°C for 2 h and reduced in flowing $H_2$ (100 ml $min_{-1}$) at 400°C for 3 h. Metal dispersions of SAPO-5 and SAPO-11, containing 0.50 wt% platinum, were estimated by $H_2$ pulse chemisorption at room temperature on a Micromeritics TPD/TPR 2900 apparatus.

Details of the characterization of SAPO-5 and SAPO-11 have been reported elsewhere (14). The surface area, $S_{BET}$, micropore volume, $V_{\mu p}$, micropore area, $S_{\mu p}$, specific metal surface area, $S_{Pt}$, and metal dispersion, $D$, are presented in Table 1.

### *Surface Acidity Measurements*

The surface acidity (sum of Brønsted and Lewis acid sites) was measured in a dynamic mode by means of the gas-phase adsorption of pyridine (PY) and 2,6-dimethylpyridine (DMPY) using a pulse-chromatographic technique according to a method described elsewhere (15, 16). A number of pulses (maintaining the same pulse size) of a given probe molecule–cyclohexane solution (approximately 1 *M*) were injected one after another into the catalyst bed in order to saturate the irreversible adsorption sites on the catalyst with the adsorbate. The pulse size was in the range 0.1 to 0.5 monolayers in order to avoid difficulties if the adsorption was not rapid and to obtain a more precise detection of effluent peaks. After saturation, different amounts of titrant were injected to calibrate the FID response. The detector (FID) response was found to be linear over the whole injection range employed in the pulse experiments. The catalyst (100 to 200 mg) was held by small plugs of Pyrex glass wool in the 4-mm-i.d. stainless-steel microreactor tube and, before each run, the catalyst samples were standardized in a stream of 12 ml $min^{-1}$ of dehydrated and deoxygenated nitrogen (99.999% pure) at 200°C for 1 h. It was also confirmed that the contribution of glass wool is negligible. The acidity measurements were repeated several times and good reproducibility of the results was obtained.

**TABLE 1**

**Physicochemical Characteristics of Pt/SAPO Catalysts**

| Catalyst | $S_{BET}$ ($m^2$ $g^{-1}$) | $V_{\mu p}$ ($cm^3$ $g^{-1}$) | $S_{\mu p}$ ($m^2$ $g^{-1}$) | Metallic area ($m^2$ $g^{-1}$) | $D$ (%) |
|---|---|---|---|---|---|
| SAPO-5 | 214 | 0.079 | 146 | — | — |
| SAPO-11 | 123 | 0.030 | 58 | — | — |
| Pt/SAPO-5 | 182 | 0.047 | 87 | 187 | 76 |
| Pt/SAPO-11 | 103 | 0.020 | 36 | 113 | 46 |

### *Catalytic Activity Measurements*

*n*-Heptane (Aldrich, >99 mol% purity) was used as a reactant. The experiments were carried out in a flow reactor system incorporating a ¼-in.-i.d. stainless-steel tubular reactor with a normal catalyst charge of 120 mg. Liquid hydrocarbon feed was pumped into a feed system vaporizer via a syringe pump (Harvard Model 4400), mixed with hydrogen flow (25 $cm^3$ $min^{-1}$) at 150°C, and fed to the reactor. The reactor effluent was on-line sampled through a heated six-way valve and analyzed by HRGC, equipped with 100-m length and 0.25-mm-i.d. fused silica capillary column, Petrocol DH. The products were characterized by FID after initial identification using mass spectrometry (VG Autospec). With $H_2$ as carrier gas, a column head pressure of 25 psi, and a constant oven temperature (70°C), very good separations were obtained for all components reported.

The reaction was carried out over a wide range of op-

TABLE 2

**Surface Acidity Properties of Pt/SAPO Catalysts**

| Catalyst | PY ($\mu$mol g$^{-1}$) | | DMPY ($\mu$mol g$^{-1}$) |
|---|---|---|---|
| | 300°C | 400°C | 300°C |
| Pt/SAPO-5 | 149 | 130 | 89 |
| Pt/SAPO-11 | 68 | 60 | 16 |
| SAPO-5 | 160 | 141 | 102 |
| SAPO-11 | 72 | 67 | 24 |

erating conditions: temperature, 300–450°C; liquid *n*-heptane flow rate, 0.6–3.6 cm$^3$ h$^{-1}$; total atmospheric pressure, 3 and 5 bar. In all cases, only one parameter was allowed to vary and the reaction proceeded until a steady state was established. Previous to activity measurements, the catalyst was pretreated at 400°C for 1 h in flowing hydrogen (25 cm$^3$ min$^{-1}$).

## RESULTS AND DISCUSSION

### *Surface Acidity*

Gas-chromatographic pulse techniques are able to provide acidity information at catalytic reaction temperatures. However, they are unable to distinguish Brønsted and Lewis centers unless specific basic probes are used. Thus, it is known that DMPY is selectively adsorbed on Brønsted acid sites, but not on Lewis acid centers, because of the steric hindrance of two methyl groups, whereas sterically nonhindered PY is adsorbed on both Brønsted and Lewis acid sites (17, 18). The distribution of acid sites in SAPO and Pt/SAPO catalysts is given in Table 2 as the amount of PY and DMPY adsorbed at the given temperature.

The number of strong acid sites is higher on Pt/SAPO-5 than on Pt/SAPO-11, according to Table 2. On the other hand, Pt/SAPO-5 presents more Brønsted acid centers than Pt/SAPO-11. However, the molecular diameter of DMPY (0.64 nm) indicates that this molecule cannot diffuse through the SAPO-11 pores, and the adsorption must occur with OH groups located either at the outer surface or near the pore ends. So the access of DMPY to the SAPO-11 pores is restricted, resulting in decreased adsorption values. In any case, Pt/SAPO-5 exhibits the highest density of acid centers, which ought to make this catalyst the most active for cumene dealkylation (14). The same behaviour is found for SAPO-5 and SAPO-11 catalysts and nearly the same values are obtained, so Pt deposition does not practically affect the distribution of acid sites.

### *Activity Results*

If the hydroconversion of *n*-heptane is taken as a probe reaction, the main steps in that catalytic hydroconversion are cracking on the strong acid sites and dehydrogenation on metallic sites. In addition, the *n*-heptene generated by dehydrogenation undergoes isomerization to isoheptanes on acid sites. Moreover, isoheptenes undergo hydrogenation to isoalkanes on metallic sites or cracking on acid sites. Furthermore, if adjacent pairs of acid–base sites are present, *n*-heptene undergoes cyclization and aromatization reactions, generating toluene.

(*a*) *Effect of reaction temperature.* The typical dependence of *n*-heptane transformation on reaction temperature both with Pt/SAPO-5 and with Pt/SAPO-11 is presented in Table 3. The catalyst has a marked effect on the distribution of both isomerization and cracking products; however, the same products are formed on all catalysts. They can be classified into three families:

(a) Methylhexanes (2-$MC_6$ and 3-$MC_6$) and ethylpentane (3-$EC_5$): monobranched isomers.

(b) Dimethylpentanes (2,2-$DMC_5$, 2,3-$DMC_5$, 3,3-$DMC_5$, and 2,4-$DMC_5$) and 2,2,3-trimethylbutane (2,2,3-$TMC_4$): multibranched isomers.

(c) Light alkanes $C_1$–$C_6$: cracked products, mainly butane fractions and propane in equimolar amounts.

The amount of cyclization and aromatization products were negligible. Furthermore, there was no formation of products heavier than $C_7$.

With Pt/SAPO-11 catalyst, isomerization is the major reaction in all temperature ranges, but as the reaction severity increases, it passes through a maximum, due to the consumption of isomerized products in consecutive hydrocracking reactions. With Pt/SAPO-5 isomerization is the major reaction only at low reaction temperatures, and the largest isoheptane conversion is about 42 wt%; at higher temperatures, cracking is the main reaction. Thus, Table 3 shows for all catalysts that the ratios of isomerized to cracked *n*-heptane, on the one hand, and of monobranched to multibranched isomers, on the other, decrease when conversion increases. This suggests that *n*-heptane is transformed successively into isomers and into cracking products, the isomerization leading to monobranched and then to multibranched isomers. Isomers are the only primary products.

Unimpregnated SAPO-5 and SAPO-11 catalysts were examined for *n*-heptane conversion. The activities of these catalysts indcate that deactivation is an important process (at 375°C, the SAPO-5 deactivated to about 70% of the initial activity over a 5-h period while the deactivation of SAPO-11 over the same time period was about 50%). Visual inspection of SAPOs catalysts indicated significant coke formation and the dramatic loss of activity is suggestive of pore plugging. In addition, initial activity and isoheptane selectivity were very low compared to those for Pt/SAPO catalysts.

The yield and distribution of heptane isomers needed

TABLE 3

*n*-Heptane Conversion over Pt/SAPO-5 and Pt/SAPO-11 Catalysts[a]

| | Pt/SAPO-5 | | | | | Pt/SAPO-11 | | | | |
|---|---|---|---|---|---|---|---|---|---|---|
| Products[b] | 300°C | 325°C | 350°C | 363°C | 400°C | 300°C | 325°C | 350°C | 400°C | 425°C |
| $C_1$ | — | 0.03 | 0.06 | 0.08 | 0.22 | — | 0.02 | 0.04 | 0.23 | 0.04 |
| $C_2$ | — | 0.05 | 0.11 | 0.13 | 0.46 | 0.02 | 0.06 | 0.13 | 0.65 | 1.10 |
| $C_3$ | 0.33 | 0.98 | 5.69 | 13.57 | 38.66 | 0.11 | 0.27 | 0.61 | 2.32 | 3.92 |
| *i*-$C_4$ | 0.13 | 0.87 | 6.67 | 16.15 | 43.36 | — | — | 0.04 | 0.43 | 0.95 |
| *n*-$C_4$ | 0.29 | 0.42 | 1.00 | 2.05 | 8.04 | 0.14 | 0.31 | 0.75 | 2.53 | 4.03 |
| *i*-$C_5$ | 0.08 | 0.12 | 0.28 | 0.60 | 1.57 | — | — | 0.02 | 0.16 | 0.39 |
| *n*-$C_5$ | 0.06 | 0.10 | 0.21 | 0.27 | 0.84 | 0.04 | 0.10 | 0.27 | 0.98 | 1.49 |
| *i*-$C_6$ | — | 0.05 | 0.20 | 0.39 | 1.09 | — | — | — | 0.17 | 0.45 |
| *n*-$C_6$ | — | 0.05 | 0.20 | 0.18 | 0.34 | 0.04 | 0.07 | 0.18 | 0.58 | 0.80 |
| 2.2-$DMC_5$ | — | 0.46 | 1.60 | 1.56 | 0.23 | — | — | — | — | 0.06 |
| 2.4-$DMC_5$ | 0.18 | 0.88 | 2.27 | 2.07 | 0.25 | — | — | 0.05 | 0.35 | 0.64 |
| 2.2.3-$TMC_4$ | — | 0.05 | 0.29 | 0.33 | 0.16 | — | — | — | — | — |
| 3.3-$DMC_5$ | — | 0.29 | 1.10 | 1.08 | 0.18 | — | — | — | — | 0.05 |
| 2.3-$DMC_5$ | 0.30 | 1.45 | 3.60 | 7.30 | 0.34 | — | — | 0.07 | 0.55 | 0.99 |
| 2-$MC_6$ | 2.84 | 8.30 | 14.34 | 12.22 | 1.13 | 0.56 | 1.86 | 4.90 | 16.34 | 19.91 |
| 3-$MC_6$ | 3.42 | 9.59 | 16.62 | 14.76 | 1.40 | 0.33 | 1.19 | 3.43 | 14.53 | 19.59 |
| 3-$EC_5$ | 0.27 | 0.79 | 1.44 | 1.27 | 0.14 | — | — | — | — | — |
| Other | 0.05 | 0.09 | 0.20 | 0.42 | — | — | 0.04 | 0.06 | 0.74 | 1.89 |
| *n*-$C_7$ | 92.05 | 75.43 | 44.12 | 25.57 | 1.59 | 98.76 | 96.08 | 89.45 | 59.44 | 43.70 |
| Total | 100 | 100 | 100 | 100 | 100 | 100 | 100 | 100 | 100 | 100 |

[a] Catalyst weight, 120 mg; $H_2$ pressure, 5 bar; *n*-heptane flow, 1.8 $cm^3\ h^{-1}$.

[b] Conversion wt%; $MC_6$, methylhexanes; $DMC_5$, dimethylpentanes; $TMC_4$, trimethylbutanes; $EC_5$, ethylpentane; $C_1$–$C_6$, alkanes from methane to hexane; other, including toluene and methylcyclohexane.

to be considered, since the industrial application of this reaction is aimed at the improvement of octane number in gasoline. The RON increases according to the sequence *n*-heptane < methylhexane < dimethylpentanes. Therefore, an ideal catalyst should be designed for high yields of dibranched isomers and high catalytic activity. Figure 1 shows molar distribution of heptane isomers with temperature, obtained for Pt/SAPO-5 and Pt/SAPO-11, according to their branching grade and monobranching distribution. As a general result, all possible *n*-heptane isomers are produced with Pt/SAPO-5. As the reaction severity increases, the content of dibranched and tribranched isomers increases, but in all cases the monobranched isomers are predominant. Isomer products obtained with Pt/SAPO-11 were monobranched (small amounts of dibranched isomers appear only at high conversions), indicating diffusional limitations in the one-dimensional porous framework of SAPO-11 (medium pore size). Moreover, on Pt/SAPO-5, whatever the conversion, 2- and 3-methylhexanes are formed in a ratio close to thermodynamic equilibrium, while on Pt/SAPO-11 this does not occur. The distribution of isomerized products as a function of the conversion degree can be explained in view of a carbocation mechanism by the relative reactivity of these isomers for further isomerization, and, most importantly, for hydrocracking. Figure 2 shows temperature dependence in cracked products distribution with both catalysts. In all cases, the propane and butane fractions in equimolar proportions are the main cracking products obtained, the isobutane/*n*-butane ratio being much higher in Pt/SAPO-5 than in Pt/SAPO-11. As a general result, the *i*-alkane/*n*-alkane ratio in cracked products is higher with Pt/SAPO-5.

On the other hand, the conversion of *n*-heptane over Pt/SAPO-5 and Pt/SAPO-11 catalysts is a first-order kinetic process. Table 4 gives the rate constants, $k$, for both catalysts at 300 and 400°C, from $\ln[1/(1 - X)]$ vs $F^{-1}$, and the activation energies, $E_a$, obtained through the Arrhenius equation by plotting $\ln k$ vs $T^{-1}$ (Fig. 3). As shown in Table 4, the catalytic activity of Pt/SAPO-5 catalyst is higher (about seven times) than the activity of Pt/SAPO-11.

(*b*) *Effect of hydrogen partial pressure.* The influence of hydrogen pressure was investigated at atmospheric pressure and at 3 and 5 bars. Figure 4 shows global *n*-heptane conversion and isomer selectivity with Pt/SAPO-5 and Pt/SAPO-11, at 375°C, as a function of reaction time. We can see that as $H_2$ pressure increases, catalyst stability becomes greater. One of the characteristics of flow reactions is that greater reactive quantities come into contact with catalysts. This causes the catalyst that undergoes deactivation to have a higher weight. In addition, in *n*-alkanes hydrocon-

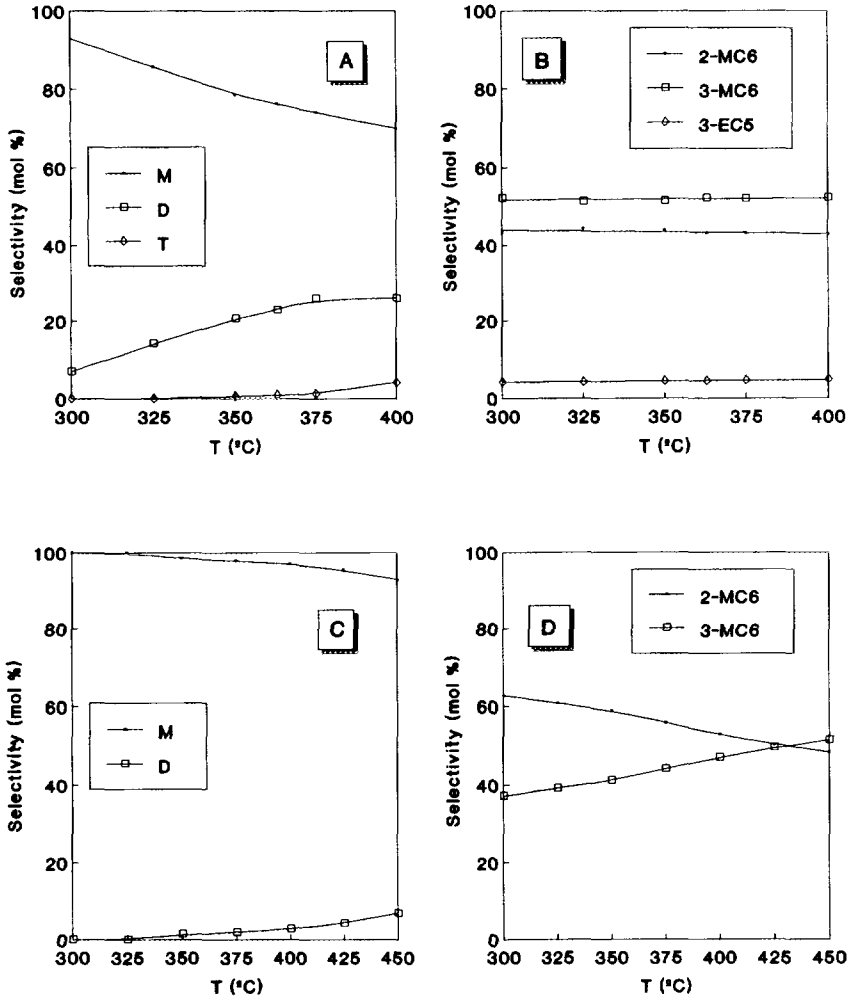


FIG. 1. Molar distribution of heptane isomers vs temperature with Pt/SAPO-5 and Pt/SAPO-11, according to their branching grade (A and C, respectively) and monobranching distribution (B and D, respectively). Conditions: 5 bar; 120 mg of catalyst; $H_2$ flow, 25 $cm^3$ $cm^{-1}$; *n*-heptane flow, 30 $\mu$l $min^{-1}$. M, monobranched isomers; D, dibranched isomers; T, tribranched isomers.

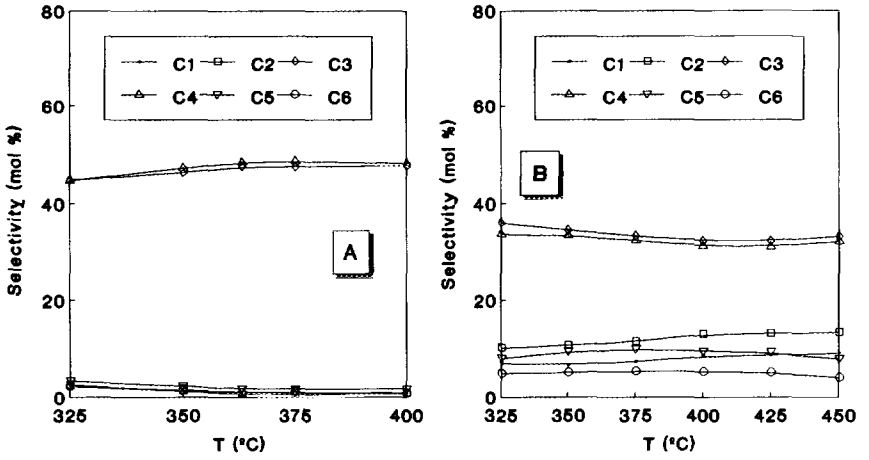


FIG. 2. Molar distribution of cracked products vs temperature with Pt/SAPO-5 (A) and Pt/SAPO-11 (B). Conditions: 5 bar; 120 mg of catalyst; $H_2$ flow, 25 $cm^3$ $min^{-1}$; *n*-heptane flow, 30 $\mu$l $min^{-1}$.

TABLE 4

**Rate Constants and Activation Energies for *n*-Heptane Hydroconversion with Pt/SAPO Catalysts**

| Catalyst | $k$, 300°C (mol $g^{-1}$ $h^{-1}$) | $k$, 400°C (mol $g^{-1}$ $h^{-1}$) | $E_a$ (kcal $mol^{-1}$) |
|---|---|---|---|
| Pt/SAPO-5 | 0.82 | 41.40 | 32.4 |
| Pt/SAPO-11 | 0.12 | 5.20 | 26.0 |

version, hydrogen pressure plays an important role in catalyst stability.

Experimental results show that we have synthesized two catalysts whose different structures impose different reactivities in *n*-heptane hydroconversion. Pt/SAPO-5 acts as an excellent *n*-heptane hydroisomerization catalyst at lower temperatures (lower conversions) while at higher temperatures no isomerization occurs. On the other hand, Pt/SAPO-11 behaves as an excellent isomerization catalyst over all temperature ranges tested, including temperatures near 450°C. On the other hand, all catalysts produce nearly the same products but in different proportions depending on their structure, reaction temperature, and Pt content.

The distribution of Pt/SAPO-5 products is very similar to that account for Pt/HY catalysts (19, 20) because they are molecular sieves with similar pore diameter. *n*-Alkane hydroconversion catalyzed by bifunctional metal/acid catalyst occurs in consecutive steps in which cracking is preceded by linear chain isomerization.

It is generally admitted that the branching of olefin intermediates occurs through protonated cyclopropane intermediates (21). This is the case for the isomerization of *n*-heptane into 2- and 3-methylhexanes, of methylhexanes into dimethylpentanes (reactions 1, 2, and 3, Fig. 5), and of dimethylpentane into trimethylbutane. With Pt/SAPO-5 catalyst, the formation of 2-methylhexane is not so favoured in relation to 3-methylhexane as in *n*-hexane isomerization (one carbonium ion of each four), but the ratio, $2\text{-}MC_6/3\text{-}MC_6$, is higher than one could expect supposing a protonated cyclopropane mechanism, PCP, and very similar to its equilibrium value. Actually it is not clear why this relation tends toward PCP value when *n*-alkane chain length increases. Since ethylpentane is a primary product with Pt/SAPO-5 and the direct transformation of *n*-heptene into ethylpentene cannot be explained with these intermediates, a rapid rearrangement by ethyl shift must be considered to explain its formation. Thus, the *n*-heptenes resulting from *n*-heptane dehydrogenation over platinum sites can undergo two reactions before hydrogenation: one through protonated cyclopropane intermediates and the other by ethyl shift.

Reactions 1, 2, 3, and 4 (Fig. 5), in which PCP intervene, can explain the isomerization of methylhexanes into dimethylpentanes. Statistical reasoning cannot account for the distribution of dimethylpentanes in the same way as for the case of methylhexanes since those carbocations are not all secondary but, in part, tertiary (hence energetically highly favoured). It can be predicted, however, that 2,3-dimethylpentane will be highly favoured since it can be formed through reactions 1, 2, and 3, whereas the other dibranched products are formed only by one of these three reactions. In addition, 2,3-dimethylpentyl carbonium ions formed in reactions 3 and 5 are tertiary, whereas the other carbocations formed are secondary. In agreement with this, formation of $2,3\text{-}DMC_5$ is greatly favoured in Pt/SAPO-5.

With Pt/SAPO-5, cracking products comprise, essentially propane and isobutane in equimolar quantities. Iso-

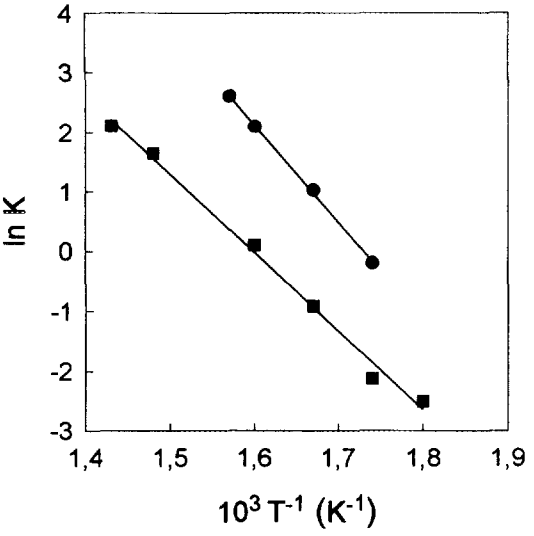


FIG. 3. Arrhenius plot for Pt/SAPO catalysts in *n*-heptane conversion: (●) SAPO-5 and (■) SAPO-11.

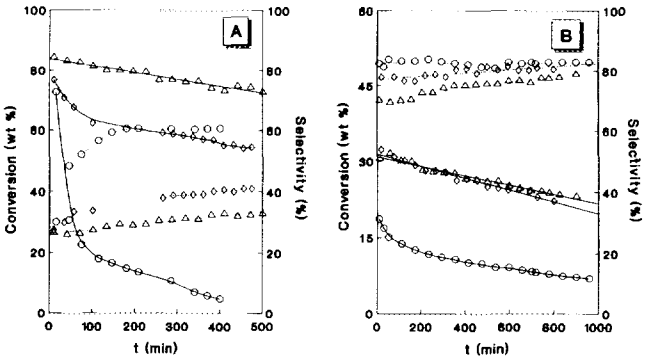


FIG. 4. Influence of hydrogen pressure in global conversion (—) and isomer selectivity (---) with Pt/SAPO-5 (A) and Pt/SAPO-11 (B) catalysts. Conditions: 120 mg of catalyst; $H_2$ flow, 25 $cm^3$ $min^{-1}$; *n*-heptane flow, 30 $\mu l$ $min^{-1}$; temperature, 375°C. $H_2$ pressure: atmospheric (○), 3 bar (◇), and 5 bar (△).

butane can be formed by cracking of tertiary 2-methylhexyl or 2,2- and 2,4-dimethylpentyl carbonium ions. Moreover, the low quantity of *n*-butane formed proves that the cracking of carbonium ions having a dimethylpentyl skeleton in which two secondary carbocations intervene is much slower. *n*-Butane can also be formed by $\beta$-scission of 2-methylhexyl or 3-methylhexyl carbocations, but these reactions involve two secondary carbocations (type C) and occur much more slowly. The $\beta$-scission of 3,3-dimethylpentane and 2,2,3-trimethylbutane, which requires the intervention of a primary carbocation, is not observed.

The selectivity of Pt/SAPO-11 catalyst is completely different from that of Pt/SAPO-5 catalyst. The amount of dibranched isomers in the products is always very low and therefore the monobranched/multibranched isomer ratio is much higher than that in Pt/SAPO-5. Moreover, bisubstituted isomers on the same carbon (2,2-dimethylpentane, 2,3-dimethylpentane, and 2,2,3-trimethylbutane), which have the highest molecular diameter, are not formed. This different isomer distribution influences cracking distribution products. So the reaction scheme is different from that found on Pt/SAPO-5 catalyst: on Pt/SAPO-5, cracking follows isomerization while on Pt/SAPO-11, some cracking products appear as the primary products. However, this does not mean only that cracking products may be the result of a direct $\beta$-scission of linear $C_7$ (type D, requires at least one primary carbonium ion), but also that hydrogenolysis takes place on Pt crystallites. This can be explained by suggesting that part of the olefinic intermediates encountered enough active acid centers to undergo successive isomerization and cracking during their migration between two plantinum sites. This can be due to a slower migration of the olefinic intermediates in the narrower pore network of Pt/SAPO-11. This structural parameter is very significant, so it is well known that molecular circulation may have a significant effect on reaction kinetics as well as on product distribution in a great number of reactions. In our case the constraints exerted by the SAPO-11 pore structure on the diffusion of the intermediate olefins would ensure a longer contact time (than in the case of SAPO-5) between the olefin and the acid sites. Moreover, the configurational limitations could also explain the low rate of formation of dibranched products: the dibranched olefins formed by isomerization of monobranched olefins would not migrate and would be transformed on site into cracking products.

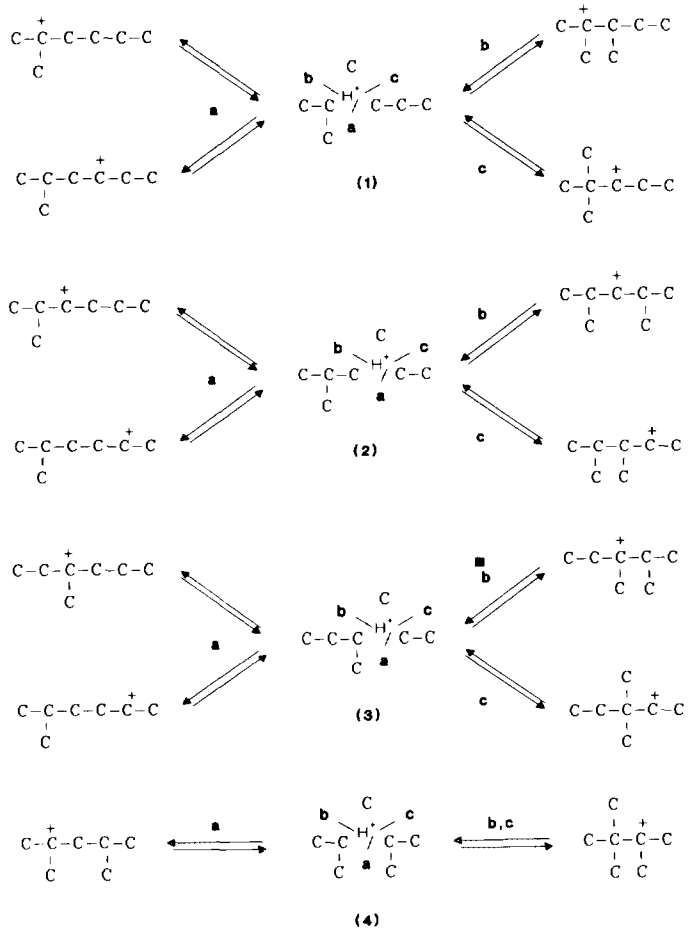


FIG. 5. Isomerization reaction mechanism involving methylhexyl, dimethylpentyl, and trimethylbutyl carbonium ions.

The distribution of monobranched isomers with Pt/SAPO-11 is very different from that found on Pt/SAPO-5 catalyst. 2-Methylhexane is highly favoured over 3-methylhexane; its formation rate is about 1.6 times greater at zero conversion. Moreover, the equilibrium between 2- and 3-methylhexanes occurs only at very high conversions. Ethylpentane is not formed. If the formation of these products involves the same steps as on Pt/SAPO-5, their relative rates must be different. The greater formation of 2-methylhexane could thus be due to a more rapid migration of 2-methylhexene than 3-methylhexene in the SAPO-11 channels (this hypothesis must be rejected because there are not significant differences between diffusional coefficients of both products) or to a faster transformation of *n*-heptyl carbonium ions into 2-methylhexyl than into 3-methylhexyl carbonium ions. This implies that some reactions are inhibited by steric constraints, which would be responsible for the fact that methylhexane interisomerization by methyl shift is slower than 2-methylhexane formation. This would explain the fact that there is no formation of ethylpentane by ethyl shift. The low amount of dimethylpentanes in the products could be due not only to the configurational limitations but also to steric constraints which inhibit the formation of the bulky protonated cyclopropane involved in the isomerization of methylhexanes into dimethylpentanes.

As on Pt/SAPO-5 catalyst, cracking leads to propane and to butane fraction, in equimolar relations. However,

the *iso*-/*n*-butane ratio is much lower. These products can result from the cracking of 2- and 3-methylhexyl carbocations, $\beta$-scission type C. Most of the $\beta$-scission of dimethylpentyl carbonium ions leads to isobutane and, consequently, must not be considered.

The size of the pores, as well as the size and the shape of the space available near the acid centers, can thus determine, in large part, the selectivity of *n*-heptane transformation in bifunctional Pt/SAPO catalysts. The differences in selectivity between Pt/SAPO-5 and Pt/SAPO-11 samples can thus be explained by the slow migration of olefinic intermediates in the SAPO-11 channels and by steric constraints.

Certainly the diffusional behaviour will also be related to configurational influences. Qualitative prediction of the diffusion of molecules in medium-pore zeolites can be made by comparing the critical molecular diameter of the sorbates to the zeolite pore diameter (22). This is defined as the smallest cylinder which can enclose the molecule in its most favourable equilibrium configuration. The critical molecular diameters are 0.49 nm for *n*-heptane, 0.56 nm for monobranched isomers and isomers dibranched over different carbon atoms, and 0.70 nm for isoheptanes dibranched over the same carbon atom. Comparison of these with the elliptical channels of SAPO-11 ($0.39 \times 0.64$ nm) indicates clearly that the lowest diffusional restriction is for the *n*-alkane; further, in comparison with the other $C_7$ hydrocarbons, those dibranched over the same carbon atom exhibit stronger diffusional retardation because of their greater molecular diameter and their lower flexibility. Consequently they appear only in trace amounts at high conversions). The presence of steric restrictions due to the SAPO-11 structure leads to a general suppression of highly branched intermediates in cracked products.

## CONCLUSIONS

In summary, the reaction schemes for *n*-heptane transformation on Pt/SAPO-5 and Pt/SAPO-11 catalysts are not the same because of their different structures. The composition of the branched isomerization and cracking products obtained on these bifunctional catalysts provides a wealth of information on the intracrystalline pore architecture. In addition, hydrogen pressure strongly influences the reaction: a strong decrease in conversion on time on stream is observed at atmospheric pressure due to the formation of cabonaceous deposits. However, the catalysts have a long life under 5 bar of hydrogen pressure since no significant changes either in activity or in selectivity occurred on time on stream.

## ACKNOWLEDGMENTS

The authors acknowledge a subsidy received from REPSOL PETROLEO S.A. Characterization of reaction products was carried out in the Mass Spectrometry Service of Corboda University.

## REFERENCES

1. Alvarez, F., Ribeiro, F. R., Giannetto, G., Chevalier, F., Perot, C., and Guisnet M., *in* "Zeolites: Facts, Figure, Future" (P. A. Jacobs and R. A. van Santen, Eds.), p. 1339. Elsevier, Amsterdam, 1989.
2. Csicsery, S. M., *Zeolites* **4,** 202 (1984).
3. Weitkamp, J., *Ind. Eng. Chem. Prod. Res. Dev.* **21,** 550 (1984).
4. Szostak, R., *in* "Molecular Sieves: Principles of Synthesis and Identification." Van Nostrand–Reinhold, New York, 1989.
5. Lok, B. M., Messina, C. A., Patton, R. L., Gajek, R. T., Cannan, T. R., and Flanigen, E. M., *J. Am. Chem. Soc.* **106,** 6092 (1984).
6. Flanigen, E. M., Patton, R. L., and Wilson, S. T., *in* "Innovation in Zeolite Materials Science" (P. J. Grobet, W. J. Mortier, E. F. Vansant, and G. Schulz-Ekloff, Eds.), p. 13. Elsevier, Amsterdam, 1988.
7. Hasha, D., Saldarriaga, L., Hataway, P. E., Cox, D. F., and Davis, M. E., *J. Am. Chem. Soc.* **110,** 2127 (1988).
8. Thomson, R. T., Wolf, E. E., Montes, C., and Davis, M. E., *J. Catal.* **124,** 401 (1990).
9. Thomson, R. T., Noh, M. M., and Wolf, E. E., *Am. Chem. Soc. Symp. Ser.* **437,** 75 (1990).
10. Choung, S. J., and Butt, J. B., *Appl. Catal.* **64,** 173 (1990).
11. Halik, C., Chaudry, S. N., and Lercher, J. A., *J. Chem. Soc. Faraday Trans. 1* **85,** 3879 (1989).
12. Martens, J. A., Grobet, P. J., and Jacobs, P. A., *J. Catal.* **126,** 289 (1990).
13. Hoffmeister, M., and Butt, J. B., *Appl. Catal. A* **82,** 169 (1992).
14. Campelo, J. M., Lafont, F., and Marinas, J. M., *in* "Proceedings, 13th Iberoamerican Symposium on Catalysis," Vol. 2, p. 1031. Segovia, Spain, 1992.
15. Ghosh, A. K., and Curthoys, G., *J. Chem. Soc. Faraday Trans. 1* **79,** 2569 (1983).
16. Campelo, J. M., Garcia, A., Luna, D., and Marinas, J. M., *J. Mater. Sci.* **25,** 2513 (1990).
17. Benesi, H. A., *J. Catal.* **28,** 176 (1973).
18. Corma, A., Rodellas, C., and Fornes, V., *J. Catal.* **88,** 374 (1984).
19. Giannetto, G., Perot, G., and Guisnet, M., *Ind. Eng Chem. Prod. Res. Dev.* **25,** 481 (1986).
20. Guisnet, M., Alvarez, F., Giannetto, G., and Perot, G., *Catal. Today* **1,** 415 (1987).
21. Brouwer, D. M., and Hogeveen, H., *in* "Progress in Physical Organic Chemistry" (A. Streitwieser, Jr., and R. W. Taft, Eds.), p. 179. Interscience, New York, 1972.
22. Choudhary, V. R., and Akolekar, D. B., *J. Catal.* **117,** 541 (1989).